

Environment-aware Near-field UE Tracking under Partial Blockage and Reflection

Hyunwoo Park, *Graduate Student Member, IEEE*, Hyeon Seok Rou, *Member, IEEE*,
Giuseppe Thadeu Freitas de Abreu, *Senior Member, IEEE*, and Sunwoo Kim, *Senior Member, IEEE*

Abstract—This paper proposes an environment-aware near-field (NF) user equipment (UE) tracking method for extremely large aperture arrays. By integrating known surface geometries and tracking the line-of-sight (LOS) and non-line-of-sight (NLOS) indicators per antenna element, the method captures partial blockages and reflections specific to the NF spherical-wavefront regime, which are unavailable under the conventional far-field (FF) assumption. The UE positions are tracked by maximizing the cosine similarity between the predicted and received channels, enabling tracking even under complete LOS obstruction. Simulation results confirm that increasing environment-awareness improves accuracy, and that NF consistently outperforms FF baselines, achieving a 0.22 m root-mean-square error with full environment-awareness.

Index Terms—Environment-awareness, near-field, tracking, partial blockage, partial reflection.

I. INTRODUCTION

NEXT-GENERATION wireless networks are envisioned not merely as communication pipelines but as perceptive infrastructures that support physical artificial intelligence (AI) systems such as autonomous vehicles, drones, and robots [1], [2]. Integrated sensing and communication (ISAC) serves as a cornerstone of this vision, enabling the network to simultaneously transfer data and extract physical-world information from radio signals [3].

Among diverse sensing functionalities, accurate user equipment (UE) positioning stands out as a fundamental enabler of location-aware resource management, predictive beam alignment, and autonomous mobility support [4], [5]. In practice, however, reliable positioning is hindered by the complex propagation environment, where surrounding surfaces cause signal blockage and multipath reflections [6].

In view of such challenging radio environments, the rapid advancement of digital twin technologies has opened a promising avenue by providing detailed environment geometry including the locations, orientations, and material properties of surrounding surfaces [7]–[9]. Leveraging such information, several recent studies have proposed localization methods that predict and incorporate the multipath propagation via ray-tracing, voxelation, and radio fingerprinting, turning reflected paths into useful position-related observations [10]–[12].

Manuscript received month day, 2026; revised month day, year. The fundamental research described in this paper was supported by the National Research Foundation of Korea under Grant NRF2023R1A2C3002890.

(Corresponding author: Sunwoo Kim)

Hyunwoo Park and Sunwoo Kim are with the Department of Electronic Engineering, Hanyang University, Seoul 04763, South Korea (e-mail: stark95@hanyang.ac.kr; remero@hanyang.ac.kr).

Hyeon Seok Rou and Giuseppe Thadeu Freitas de Abreu are with the School of Computer Science and Engineering, Constructor University Bremen, 28759 Bremen, Germany (e-mail: hrou@constructor.university; gabreu@constructor.university).

Nevertheless, these approaches predominantly rely on far-field (FF) channel models and assume that intermediate parameters such as time-of-arrival (TOA) and angle-of-arrival (AOA) have already been extracted prior to position estimation [13], inherently limiting their applicability since the extraction step itself requires accurate path-level modeling that becomes increasingly difficult under complex propagation conditions.

Amidst these bottlenecks, a key trend emerged which fundamentally reshaped the propagation landscape – the deployment of extremely large aperture arrays (ELAAs) at high-frequency bands, substantially extending the near-field (NF) region governed by the spherical wavefront model [14]–[16]. In the NF regime, a single surface may block or reflect the signal for only a subset of antenna elements, giving rise to partial blockage and partial reflection unique to spherical-wavefront propagation [17], [18]. These spatially-selective effects violate the all-or-nothing path model inherent to FF channel parameter estimation, rendering existing environment-aware methods inadequate for NF systems.

Recent NF localization and tracking works have begun to account for such partial effects [19]–[21], however, they do not incorporate environment geometry and thus cannot predict reflection paths or model blockage from surfaces outside the direct line-of-sight (LOS) path. Conversely, existing environment-aware approaches [10], [12], [13] rely on FF models that inherently cannot capture per-element partial effects. A method that jointly exploits environment geometry and NF propagation characteristics therefore remains unexplored.

In light of the above, this paper addresses the aforementioned gap by proposing an environment-aware NF UE tracking method that directly estimates the UE position from the received signal, bypassing conventional channel parameter extraction. To the best of the authors’ knowledge, this is the first work to jointly embed known surface geometries into a per-antenna-element NF channel prediction framework for UE tracking. The main contributions are summarized as follows:

- A per-element channel prediction framework is developed which incorporates surface geometries to determine individual LOS and NLOS conditions. This captures partial blockage and reflection effects unique to the NF spherical-wavefront regime, which are unmodeled under conventional FF planar-wavefront assumptions.
- A cosine-similarity-based estimator is formulated, which is invariant to unknown transmit power and pilot phase. By exploiting predicted reflections from known surfaces, the method enables continuous UE tracking even under complete LOS obstruction.

Notations: Vectors and matrices are written in lower- and upper- case bold letters respectively and sets by calligraphic

font. For example, a vector, a matrix, and a set are denoted by \mathbf{a} , \mathbf{A} and \mathcal{A} , respectively. Superscripts $(\cdot)^H$ denotes Hermitian transpose, $\iota = \sqrt{-1}$ is the imaginary unit, and $\|\cdot\|$ returns the Euclidean norm.

II. UE TRACKING SYSTEM AND PROBLEM FORMULATION

A. UE Tracking System

Consider a scenario in which a mobile single-antenna UE communicates with an ELAA base station (BS) equipped with N antennas. A two-dimensional (2D) environment is considered, containing S surfaces that partially reflect or block signal paths – each modeled as a line segment¹. The BS is assumed to have knowledge of a subset (up to a complete set) of these surfaces and tracks the UE's position by receiving its uplink signals.

Let \mathcal{S} denote the set of all S surfaces and $\mathcal{S}_a \subseteq \mathcal{S}$ denote the subset of S_a surfaces known to the BS. The environment-awareness level is defined as the ratio $\eta = S_a/S \in [0, 1]$, representing the fraction of surfaces whose geometry is available at the BS.

At time k , the uplink signal $\mathbf{z}_{k,m} \in \mathbb{C}^{N \times 1}$ received at the BS on the m -th subcarrier is expressed as

$$\mathbf{z}_{k,m} = \sqrt{\frac{P}{M}} \mathbf{h}_m(\mathbf{p}_k) x_{k,m} \exp(\iota \phi_{k,m}) + \mathbf{w}_{k,m} \quad (1)$$

where P is the transmit power of the UE, M is the number of subcarriers, $\mathbf{h}_m(\mathbf{p}_k) \in \mathbb{C}^{N \times 1}$ denotes the channel vector from the UE at position \mathbf{p}_k to the BS, $x_{k,m}$ is the unit-power transmitted pilot symbol, $\phi_{k,m}$ is the phase error caused by imperfect synchronization between the UE and the BS, and $\mathbf{w}_{k,m} \sim \mathcal{CN}(\mathbf{0}_N, \sigma_w^2 \mathbf{I}_N)$ represents the additive white Gaussian noise (AWGN). The noise variance per subcarrier is $\sigma_w^2 = k_B T \Delta_f F$, where k_B is the Boltzmann constant, T the ambient temperature, Δ_f the subcarrier spacing, and F the noise figure.

The channel vector $\mathbf{h}_m(\mathbf{p}_k)$ will capture both LOS and non-line-of-sight (NLOS) propagation paths, including reflections from surrounding surfaces. For tractability, this paper considers specular reflections from smooth surfaces, where the reflection coefficient follows the Fresnel equations [22]. Considering single-bounce propagation, which is well justified since higher-order reflections are negligible relative to the noise floor at the considered frequency [23], the set of paths reaching the n -th antenna element is characterized using \mathcal{S} .

Next, define the LOS path indicator for the n -th antenna element as

$$b_n^{\text{LOS}}(\mathbf{p}; \mathcal{S}) = \begin{cases} 1 & \text{if } \overline{\mathbf{p}'_n \mathbf{p}} \cap s = \emptyset, \forall s \in \mathcal{S} \\ 0 & \text{otherwise} \end{cases} \quad (2)$$

where $\overline{\mathbf{p}'_n \mathbf{p}}$ denotes the line segment connecting the n -th antenna position \mathbf{p}'_n and the UE position \mathbf{p} , in other words, the indicator b_n^{LOS} returns a value of 1 only if the LOS path between \mathbf{p}'_n and \mathbf{p} does not intersect with any surface in \mathcal{S} .

Similarly, each surface $s \in \mathcal{S}$ can potentially generate a reflection path. The reflection point $\mathbf{r}_{n,s}(\mathbf{p})$ on surface s for

the n -th antenna is computed via the image method [24], and the resulting path is considered valid if (i) the reflection point lies within the finite extent of surface s , and (ii) neither the incident nor the reflected segment is blocked by any other surface in \mathcal{S} . Then, NLOS path indicator for surface s is defined as

$$b_{n,s}^{\text{NLOS}}(\mathbf{p}; \mathcal{S}) = \begin{cases} 1 & \text{if conditions (i) and (ii) hold,} \\ 0 & \text{otherwise.} \end{cases} \quad (3)$$

In all, the set of propagation paths for the n -th antenna is given by

$$\mathcal{L}_n(\mathbf{p}; \mathcal{S}) = \{0 \text{ if } b_n^{\text{LOS}} = 1\} \cup \{s \in \mathcal{S} \text{ if } b_{n,s}^{\text{NLOS}} = 1\} \quad (4)$$

where the index 0 denotes the LOS path. Note that both the number of propagation paths $|\mathcal{L}_n|$ and the positions of reflection points $\mathbf{r}_{n,s}(\mathbf{p})$ differ for each antenna element due to NF effects, which induce partial blockage and partial reflection. Furthermore, the n -th element of the channel vector is expressed as

$$h_{m,n}(\mathbf{p}) = \sum_{l \in \mathcal{L}_n(\mathbf{p}; \mathcal{S})} \frac{\beta_{m,l}(\mathbf{p})}{\sqrt{\alpha_{m,n,l}(\mathbf{p})}} \exp\left(-\iota \frac{2\pi}{\lambda_m} d_{n,l}(\mathbf{p})\right) \quad (5)$$

where $\beta_{m,l}(\mathbf{p}) \in [0, 1]$ is the reflection coefficient with $\beta_{m,0}(\mathbf{p}) = 1$ for LOS, and $\alpha_{m,n,l}(\mathbf{p})$ is the path loss.

The path loss follows [23]

$$\alpha_{m,n,l}(\mathbf{p}) = \left(\frac{4\pi}{\lambda_m} d_{n,l}(\mathbf{p})\right)^2 \quad (6)$$

where λ_m is the wavelength for the m -th subcarrier and $d_{n,l}(\mathbf{p})$ is the total propagation distance of the l -th path associated with the n -th antenna element and position \mathbf{p} .

The propagation distance $d_{n,l}(\mathbf{p})$ is expressed as

$$d_{n,l}(\mathbf{p}) = \begin{cases} \|\mathbf{p}'_n - \mathbf{p}\| & \text{if } l = 0 \text{ (LOS)} \\ \|\mathbf{p}'_n - \mathbf{r}_{n,l}(\mathbf{p})\| + \|\mathbf{r}_{n,l}(\mathbf{p}) - \mathbf{p}\| & \text{if } l = s \text{ (NLOS)} \end{cases} \quad (7)$$

B. Problem Formulation

The objective of the presented problem is to track the UE position by exploiting environment geometry information alongside the received uplink signals. Given knowledge of the surface subset \mathcal{S}_a , the propagation paths can be predicted for any candidate UE position \mathbf{p} by evaluating (2)–(5) with \mathcal{S}_a in place of \mathcal{S} . The predicted channel vector $\hat{\mathbf{h}}_m(\mathbf{p}; \mathcal{S}_a) \in \mathbb{C}^{N \times 1}$ whose n -th element is expressed as

$$\hat{h}_{m,n}(\mathbf{p}; \mathcal{S}_a) = \sum_{l \in \mathcal{L}_n(\mathbf{p}; \mathcal{S}_a)} \frac{\beta_{m,l}(\mathbf{p})}{\sqrt{\alpha_{m,n,l}(\mathbf{p})}} \exp\left(-\iota \frac{2\pi}{\lambda_m} d_{n,l}(\mathbf{p})\right) \quad (8)$$

which shares the same functional form as the true channel in (5) but is evaluated over the path set $\mathcal{L}_n(\mathbf{p}; \mathcal{S}_a)$ determined by the known surfaces only. Trivially, when $\eta = 1$ (i.e., $\mathcal{S}_a = \mathcal{S}$), the predicted path set coincides with the true path set, such that $\hat{\mathbf{h}}_m(\mathbf{p}; \mathcal{S}) = \mathbf{h}_m(\mathbf{p})$.

¹The proposed per-element path evaluation extends directly to three-dimensional (3D) environments by replacing line-segment intersection tests with ray-polygon tests at the same asymptotic complexity.

A tracking scenario is considered in which the initial UE position \mathbf{p}_0 is assumed to be known. At time k , given the previous position estimate $\hat{\mathbf{p}}_{k-1}$, the current position of the UE $\hat{\mathbf{p}}_k$ is estimated. Since the transmit power P and pilot symbol phase may not be known at the BS, a metric that is invariant to complex scaling is desirable. For a given measurement $\mathbf{z}_{k,1:M}$, the position estimate at time k is therefore obtained by maximizing the cosine similarity between the received signal and the predicted channel as [25]

$$\hat{\mathbf{p}}_k = \underset{\mathbf{p} \in \mathcal{R}_k}{\operatorname{argmax}} \sum_{m=1}^M \frac{|\hat{\mathbf{h}}_m^H(\mathbf{p}; \mathcal{S}_a) \mathbf{z}_{k,m}|}{\|\hat{\mathbf{h}}_m(\mathbf{p}; \mathcal{S}_a)\| \|\mathbf{z}_{k,m}\|} \quad (9)$$

where \mathcal{R}_k denotes the search space at time k , constructed from the previous position estimate $\hat{\mathbf{p}}_{k-1}$ and UE mobility constraints, as detailed in Sec. III. Since $\phi_{k,m}$ may differ across subcarriers, the cosine similarity is computed per subcarrier and its magnitude is summed, making each term individually invariant to the subcarrier-specific phase.

The predicted channel $\hat{\mathbf{h}}_m(\mathbf{p}; \mathcal{S}_a)$ inherently accounts for partial blockage and reflection effects determined by the known environment geometry, enabling accurate tracking under severe NLOS conditions. When $\eta < 1$, surfaces in $\mathcal{S} \setminus \mathcal{S}_a$ are invisible to the BS: their blockage effects cause unmodeled path attenuation, and their reflection paths are absent from the predicted channel. Both effects degrade the cosine similarity at the true UE position, leading to increased tracking error.

III. ENVIRONMENT-AWARE UE TRACKING

This section presents the proposed method for solving (9). Rather than relying on Kalman or particle filters, which require linearization that can introduce substantial model mismatch in the highly nonlinear NF channel under partial blockage, this paper directly evaluates the full channel vector at each candidate position. The approach involves two steps: constructing a tractable search space \mathcal{R}_k from UE mobility constraints, and computing the predicted channel $\hat{\mathbf{h}}_m(\mathbf{p}; \mathcal{S}_a)$ to maximize the cosine similarity.

A. Search Space Construction

The search space \mathcal{R}_k at time k is constructed based on UE mobility constraints and the previous position estimate $\hat{\mathbf{p}}_{k-1}$. Assuming the UE moves with a maximum speed v_{\max} , the search space is defined as

$$\mathcal{R}_k = \{\mathbf{p} : \|\mathbf{p} - \hat{\mathbf{p}}_{k-1}\| \leq v_{\max} \Delta_t + E\} \quad (10)$$

where Δ_t denotes the tracking time interval and E represents a margin to account for potential tracking errors from the previous time step. This formulation ensures that \mathcal{R}_k encompasses all physically reachable positions given the UE mobility constraints, while the margin E provides robustness against accumulated estimation errors.

The search space \mathcal{R}_k is discretized into a uniform grid \mathcal{G}_k with spacing Δ_g , where the grid spacing Δ_g controls the trade-off between tracking accuracy and computational complexity. Given the above, the position estimate $\hat{\mathbf{p}}_k$ is obtained as the grid point that maximizes the objective in (9) over \mathcal{G}_k .

B. Environment-aware NF UE Tracking

For each candidate grid point $\mathbf{p} \in \mathcal{G}_k$, the BS constructs the predicted channel vector $\hat{\mathbf{h}}_m(\mathbf{p}; \mathcal{S}_a)$ defined in (8) using only the known surface subset \mathcal{S}_a . The computation consists of three steps:

- **Step 1** (LOS path determination): For each antenna element n , evaluate the LOS path indicator $b_n^{\text{LOS}}(\mathbf{p}; \mathcal{S}_a)$ defined in (2) with \mathcal{S}_a in place of \mathcal{S} . The indicator equals 1 if the line segment $\overline{\mathbf{p}'_n \mathbf{p}}$ does not intersect any surface in \mathcal{S}_a , and 0 otherwise.
- **Step 2** (NLOS path determination): For each surface $s \in \mathcal{S}_a$ and antenna element n , compute the reflection point $\mathbf{r}_{n,s}(\mathbf{p})$ via the image method and evaluate the NLOS path indicator $b_{n,s}^{\text{NLOS}}(\mathbf{p}; \mathcal{S}_a)$ defined in (3) with \mathcal{S}_a in place of \mathcal{S} .
- **Step 3** (Channel vector construction): Assemble the predicted path set $\mathcal{L}_n(\mathbf{p}; \mathcal{S}_a)$ using (4) with \mathcal{S}_a , and compute $\hat{h}_{m,n}(\mathbf{p}; \mathcal{S}_a)$ via (8) for all antenna elements and subcarriers.

After the three steps, the position estimate at time k can be obtained by evaluating

$$\hat{\mathbf{p}}_k = \underset{\mathbf{p} \in \mathcal{G}_k}{\operatorname{argmax}} \sum_{m=1}^M \frac{|\hat{\mathbf{h}}_m^H(\mathbf{p}; \mathcal{S}_a) \mathbf{z}_{k,m}|}{\|\hat{\mathbf{h}}_m(\mathbf{p}; \mathcal{S}_a)\| \|\mathbf{z}_{k,m}\|} \quad (11)$$

which is the grid-discretized counterpart of (9).

Note that in contrast to the true channel vector $\mathbf{h}_m(\mathbf{p})$, which depends on all S surfaces via $\mathcal{L}_n(\mathbf{p}; \mathcal{S})$, the predicted channel accounts for blockage and reflection only through the surfaces in \mathcal{S}_a . Surfaces in $\mathcal{S} \setminus \mathcal{S}_a$ are invisible to the BS: their blockage effects on existing paths are unmodeled, and their reflection paths are absent from $\mathcal{L}_n(\mathbf{p}; \mathcal{S}_a)$.

IV. SIMULATION RESULTS AND CASE STUDIES

In this section, the proposed environment-aware NF UE tracking method is evaluated through numerical simulations. The simulated environment consists of $S = 8$ surfaces that act as reflectors and blockers under single-bounce propagation, as illustrated by the grey areas in Fig. 1. For each environment-awareness level η , the known subset \mathcal{S}_a is drawn uniformly at random from \mathcal{S} , and the tracking root-mean-square error (RMSE) is averaged over multiple realizations and all trackable UE positions. Further simulation parameters are summarized in Tab. I.

TABLE I
SIMULATION PARAMETERS.

Description	Parameter	Value
Number of antennas	N	64
Number of surfaces	S	8
Carrier frequency	f_c	7.5 GHz
Bandwidth	-	100 MHz
Subcarrier spacing	Δ_f	120 kHz
Number of subcarriers for tracking	M	16
Transmit power	P	23 dBm
Noise figure	F	7 dB
Kelvin temperature	T	290 K
Tracking interval	Δ_t	0.05 s
Maximum speed	v_{\max}	10 m/s
Error margin	E	0.5 m
Grid spacing	Δ_g	0.05 m

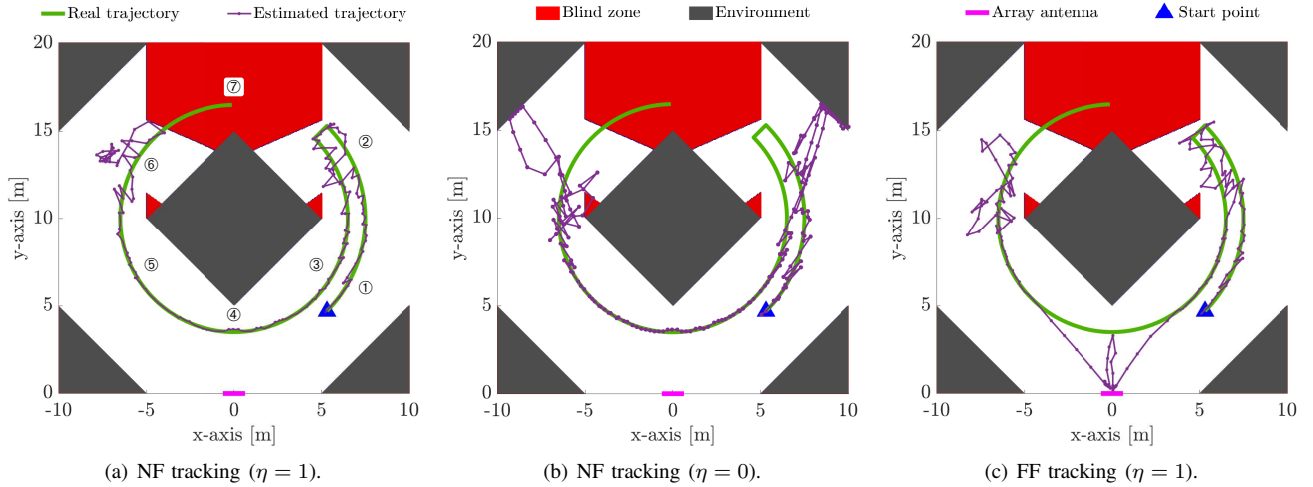


Fig. 1. Tracking trajectories under three representative conditions. The UE traverses propagation zones ① LOS+NLOS, ② NLOS, ③ LOS+NLOS, ④ LOS, ⑤ LOS+NLOS, ⑥ NLOS, and ⑦ blind zone, in order.

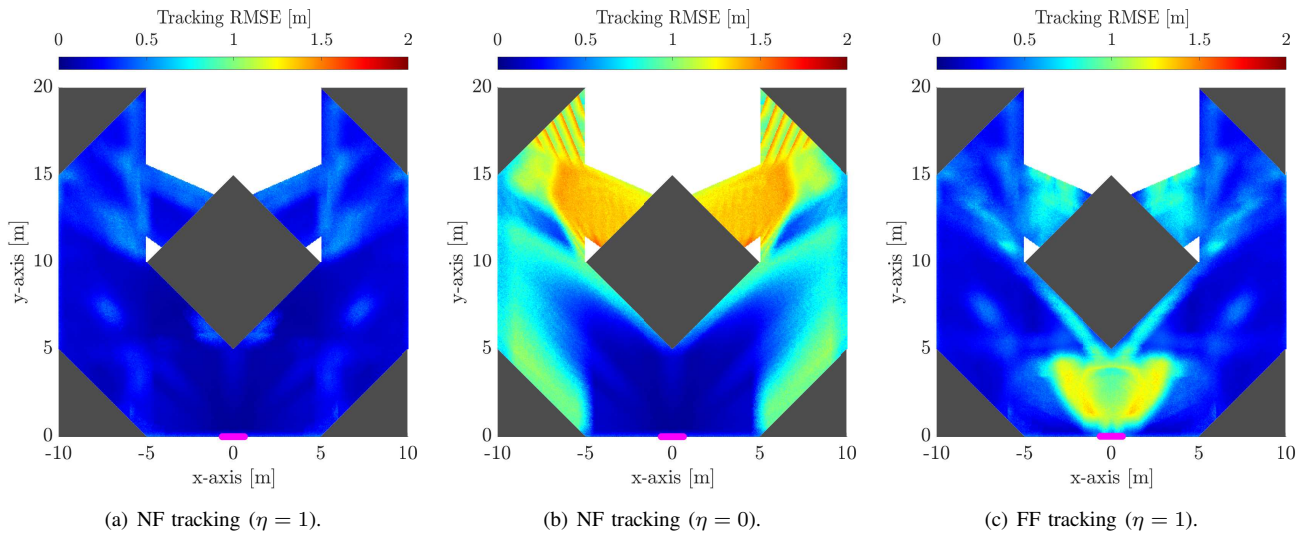


Fig. 2. Spatial distribution of tracking RMSE over the trackable area.

Two baselines are adopted for comparison. First, to isolate the gain from environment-awareness, an NF variant that performs grid search using only the LOS channel without any surface knowledge (i.e., $\eta = 0$) is considered, following the framework in [25]. Second, to isolate the gain attributable to the NF model, a FF variant that shares the identical environment-aware framework but replaces per-element path indicators with array-common ones is adopted, i.e., $b_n^{\text{LOS}}(\mathbf{p}; \mathcal{S}_a)$ and $b_{n,s}^{\text{NLOS}}(\mathbf{p}; \mathcal{S}_a)$ are constant across n , so that partial blockage and partial reflection effects are not captured.

Accordingly, Fig. 1 illustrates the tracking trajectories for the proposed method and the two baselines. With full environment knowledge under the NF model (Fig. 1(a)), the estimated trajectory closely follows the true path throughout the entire course, including regions where the LOS is completely blocked (excluding the complete blind zone), since the BS can predict reflection paths from the known surfaces and exploit them for position estimation. Without environment knowledge (Fig. 1(b)), the tracker relies solely on the LOS path for channel prediction; the estimated trajectory remains accurate in LOS-dominant regions, but degrades noticeably as the UE enters NLOS-dominant areas and fails when the LOS

is absent. Comparing Figs. 1(a) and 1(c) reveals the limitation of the FF assumption. Although full environment knowledge is available in both cases, the FF tracker (Fig. 1(c)) exhibits performance degradation at positions close to the BS and at locations where partial blockage or partial reflection occurs.

Since the planar-wavefront model assigns identical path indicators across all antenna elements, it cannot capture the spatially-selective propagation phenomena that arise under the spherical wavefront, leading to a mismatch between the predicted and true channel vectors at these positions.

In complement, Fig. 2 presents the spatial distribution of the tracking RMSE over *all* trackable positions. Under the proposed NF method with $\eta = 1$ (Fig. 2(a)), the RMSE remains below 0.45 m across the entire trackable area. When $\eta = 0$ (Fig. 2(b)), comparable accuracy is maintained in LOS-only regions, but the RMSE increases progressively as the UE enters NLOS-dominant regions where unmodeled multipath distorts the cosine similarity metric. For the FF baseline with $\eta = 1$ (Fig. 2(c)), elevated RMSE values persist near the BS and at partial blockage/reflection positions, where the all-or-nothing path model deviates from the true propagation.

Finally, Fig. 3 summarizes the average tracking RMSE as a function of the environment-awareness level η , from 0

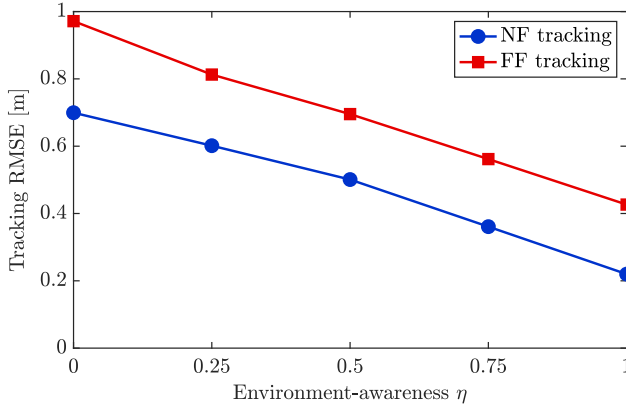


Fig. 3. Tracking RMSE versus environment-awareness level η .

to 1, for both the proposed NF and the FF methods. Both methods benefit from increasing environment-awareness, as additional surface knowledge enables more accurate channel prediction. In particular, the proposed NF method reduces the average RMSE from 0.70 m at $\eta = 0$ to 0.22 m at $\eta = 1$. Moreover, the proposed NF method consistently outperforms the FF baseline across all values of η . The performance gap persists even at $\eta = 1$, confirming that the advantage of the NF model stems not only from environment-awareness but also from the accurate modeling of partial blockage and partial reflection. These results demonstrate that incorporating both environment geometry and NF propagation characteristics into the tracking framework is essential for achieving high-accuracy UE tracking in ELAA systems.

For each candidate position $\mathbf{p} \in \mathcal{G}_k$, evaluating the LOS and NLOS indicators requires $\mathcal{O}(NS_a^2)$ intersection checks, and constructing the channel vector across M subcarriers costs $\mathcal{O}(NM(S_a+1))$. With $|\mathcal{G}_k| \approx (v_{\max}\Delta_t + E)^2/\Delta_g^2$ grid points, the total per-step complexity is $\mathcal{O}(|\mathcal{G}_k|N(S_a^2 + MS_a))$. Under the simulation parameters, the measured per-step execution time is less than 0.02 s, which is well below the tracking interval $\Delta_t = 0.05$ s, confirming real-time feasibility. The grid spacing $\Delta_g = 0.05$ m is chosen to be sufficiently fine so that it does not bottleneck the tracking accuracy.

V. CONCLUSION

This paper proposed an environment-aware NF UE tracking method that leverages known surface geometries to construct per-antenna-element channel predictions, thereby capturing partial blockage and partial reflection effects unique to the NF regime. By directly maximizing the cosine similarity between predicted and received channel vectors, the proposed method bypasses conventional channel parameter extraction and enables continuous tracking even under complete LOS obstruction. Numerical results confirmed that increasing environment-awareness progressively enhances tracking performance, and that the NF model consistently outperforms the FF baseline across all awareness levels, demonstrating the necessity of jointly exploiting environment geometry and NF propagation characteristics for high-accuracy UE tracking in ELAA systems. Future work includes extensions to 3D multi-bounce environments, multi-static placements of arrays, and robustness analysis under surface geometry uncertainties.

REFERENCES

- [1] W. Saad, M. Bennis, and M. Chen, "A vision of 6G wireless systems: Applications, trends, technologies, and open research problems," *IEEE Netw.*, vol. 34, no. 3, pp. 134–142, May 2020.
- [2] K. B. Letaief, Y. Shi, J. Lu, and J. Lu, "Edge artificial intelligence for 6G: Vision, enabling technologies, and applications," *IEEE J. Sel. Areas Commun.*, vol. 40, no. 1, pp. 5–36, Jan. 2022.
- [3] F. Liu *et al.*, "Integrated sensing and communications: Toward dual-functional wireless networks for 6G and beyond," *IEEE J. Sel. Areas Commun.*, vol. 40, no. 6, pp. 1728–1767, Jun. 2022.
- [4] M. Z. Win, Z. Wang, Z. Liu, Y. Shen, and A. Conti, "Location awareness via intelligent surfaces: A path toward holographic NLN," *IEEE Veh. Technol. Mag.*, vol. 17, no. 2, pp. 37–45, June 2022.
- [5] J. A. del Peral-Rosado *et al.*, "Survey of cellular mobile radio localization methods: From 1G to 5G," *IEEE Commun. Surveys Tuts.*, vol. 20, no. 2, pp. 1124–1148, Second Quart. 2018.
- [6] G. Torsoli, M. Z. Win, and A. Conti, "Blockage intelligence in complex environments for beyond 5G localization," *IEEE J. Sel. Areas Commun.*, vol. 41, no. 6, pp. 1688–1701, June 2023.
- [7] L. U. Khan, W. Saad, D. Niyato, Z. Han, and C. S. Hong, "Digital-twin-enabled 6G: Vision, architectural trends, and future directions," *IEEE Commun. Mag.*, vol. 60, no. 1, pp. 74–80, Jan. 2022.
- [8] A. Alkhateeb, S. Jiang, and G. Charan, "Real-time digital twins: Vision and research directions for 6G and beyond," *IEEE Commun. Mag.*, vol. 61, no. 11, pp. 128–134, Nov. 2023.
- [9] F. Tao *et al.*, "Digital twin in industry: State-of-the-art," *IEEE Trans. Ind. Informat.*, vol. 15, no. 4, pp. 2405–2415, Apr. 2019.
- [10] O. Kanhere and T. S. Rappaport, "Map-assisted millimeter wave and terahertz position location and sensing," *IEEE Trans. Wireless Commun.*, vol. 24, no. 6, pp. 5323–5336, Mar. 2025.
- [11] H. S. Rou *et al.*, "Integrated sensing and communications for 3D object imaging via bilinear inference," *IEEE Transactions on Wireless Communications*, vol. 23, no. 8, pp. 8636–8653, 2024.
- [12] J. Son *et al.*, "Transformer-based environment-aware localization in the NLoS scenarios," in *Proc. IEEE Wireless Communi. Net. Conf. (WCNC)*, Apr. 2024, pp. 1–6.
- [13] R. Mendrzik, H. Wymeersch, G. Bauch, and Z. Abu-Shaban, "Harnessing NLOS components for position and orientation estimation in 5G millimeter wave MIMO," *IEEE Trans. Wireless Commun.*, vol. 18, no. 1, pp. 93–107, Jan. 2019.
- [14] Y. Liu, Z. Wang, J. Xu, C. Ouyang, X. Mu, and R. Schober, "Near-field communications: A tutorial review," *IEEE Open J. Commun. Soc.*, vol. 4, pp. 1999–2049, 2023.
- [15] H. Imori *et al.*, "Joint activity and channel estimation for extra-large MIMO systems," *IEEE Trans. Wireless Commun.*, vol. 21, no. 9, pp. 7253–7270, Sep. 2022.
- [16] H. Imori *et al.*, "Grant-free access for extra-large MIMO systems subject to spatial non-stationarity," in *Proc. IEEE Int. Conf. Commun. (ICC)*, Seoul, Korea, pp. 1758–1762, 2022.
- [17] H. Chen, P. Zheng, Y. Ge, A. Elzanaty, J. He, T. Y. Al-Naffouri, and H. Wymeersch, "ELAA near-field localization and sensing with partial blockage detection," in *Proc. IEEE Int. Symp. Pers., Indoor Mobile Radio Commun. (PIMRC)*, Sep. 2024, pp. 1–6.
- [18] J. Xu, B. Ottersten, and A. L. Swindlehurst, "Partially-blocked near-field sensing: Joint source DoA and blockage range estimation," in *Proc. Asilomar Conf. Signals, Syst., Comput.*, Oct. 2024, pp. 1871–1875.
- [19] A. Guerra, F. Guidi, D. Dardari, and P. M. Djurić, "Near-field tracking with large antenna arrays: Fundamental limits and practical algorithms," *IEEE Trans. Signal Process.*, vol. 69, pp. 5723–5738, Aug. 2021.
- [20] H. Park, H. Chung, A. Conti, M. Z. Win, and S. Kim, "Robust near-field beam tracking via deep Q-network for THz communications," in *Proc. Int. Conf. Inf. Fusion (FUSION)*, July 2024, pp. 1–5.
- [21] H. Park, A. Conti, M. Z. Win, and S. Kim, "Towards grid-free positioning for near-field communications," in *Proc. Int. Conf. Artif. Intell. Inf. Commun. (ICAIC)*, Feb. 2025, pp. 0172–0175.
- [22] T. S. Rappaport, *Wireless communications: Principles and practice, 2/E*. Pearson Education India, 2010.
- [23] *Technical Specification Group Radio Access Network; Study on Channel Model for Frequencies From 0.5 to 100 GHz*. document TR 38.901 V18.0.0, Release 18, Mar. 2024.
- [24] Z. Yun and M. F. Iskander, "Ray tracing for radio propagation modeling: Principles and applications," *IEEE Access*, vol. 3, pp. 1089–1100, July 2015.
- [25] Z. Lu, Y. Han, S. Jin and M. Matthaiou, "Near-field localization and channel reconstruction for ELAA systems," *IEEE Trans. Wireless Commun.*, vol. 23, no. 7, pp. 6938–6953, July 2024.